Revised MS #aenm.201800014

Fabrication of Submicron-thick Solid Electrolyte Membranes of *β*-Li_3PS_4 *via* Tiled Assembly of Nanoscale, Plate-like Building Blocks

Zachary D. Hood,[1,2,†] Hui Wang,[3,†] Amaresh Samuthira Pandian,[4] Rui Peng,[1] Kyle D. Gilroy,[5] Miaofang Chi,[1,*] Chengdu Liang,[1,*] Younan Xia[2,5,6,*]

[1]*Center for Nanophase Materials Sciences, Oak Ridge National Laboratory, Oak Ridge, Tennessee, 37830, USA*

[2]*School of Chemistry and Biochemistry, Georgia Institute of Technology, Atlanta, GA, 30332, USA*

[3]*Department of Mechanical Engineering, Conn Center for Renewable Energy Research, University of Louisville, Louisville, KY, 40292*

[4]*Materials Science and Technology Division, Oak Ridge National Laboratory, Oak Ridge, Tennessee, 37830, USA*

[5]*Wallace H. Coulter Department of Biomedical Engineering, Georgia Institute of Technology and Emory University, Atlanta, GA 30332, USA*

[6]*School of Chemical and Biomolecular Engineering, Georgia Institute of Technology, Atlanta, GA 30332, USA*

[†]*These authors contributed equally to this publication*

Corresponding authors: Miaofang Chi (chim@ornl.gov), Chengdu Liang (cd_liang@hotmail.com) and Younan Xia (younan.xia@bme.gatech.edu)

ToC Entry

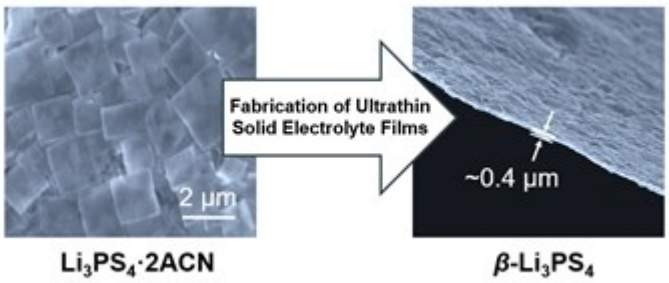

Submicron-thick membranes of *β*-Li_3PS_4, a promising solid electrolyte for Li-metal batteries, are fabricated for the first time with nanoscale, plate-like building blocks composed of Li_3PS_4·2ACN. The solid electrolyte membranes offer high ionic conductivity, good thermal stability, and compatibility with metallic lithium anode.

Keywords:

Lithium thiophosphate, shape control, solid electrolytes, solvent exfoliation, thin films

Abstract

Solid electrolytes represent a critical component in future batteries that provide higher energy and power densities than the current lithium-ion batteries. The potential of using ultrathin films is among the best merits of solid electrolytes for considerably reducing the weight and volume of each battery unit, thereby significantly enhancing the energy density. However, it is challenging to fabricate ultrathin membranes of solid electrolytes using the conventional techniques. Here we report a new strategy for fabricating submicron-thick membranes of *β*-Li_3PS_4 solid electrolytes *via* tiled assembly of shape-controlled, nanoscale building blocks. This strategy relies on facile, low-cost, solution-based chemistry to create membranes with tunable thicknesses. The ultrathin membranes of *β*-Li_3PS_4 show desirable ionic conductivity and necessary compatibility with metallic lithium anode. Our results also highlight a viable strategy for creating ultrathin, dense solid electrolytes with high ionic conductivities for the next-generation energy storage and conversion systems.

1. Introduction

The rapidly growing demand for energy storage requires new battery technologies beyond current state-of-the-art lithium-ion batteries. Among all the potential solutions, Li-metal batteries, which offer the highest specific capacity of lithium and lowest negative electrochemical potential, are expected to provide a maximized capacity density and voltage window, increasing the overall energy density for the battery.[1] While different configurations of Li-metal batteries have been proposed, including all-solid-state, Li-air, and Li-S batteries, solid electrolytes are considered one of the critical components that will enable the use of metallic lithium in most of these designs.[1a, 2] Currently, solid electrolytes can be divided into three main categories for battery-related applications: polymers, sulfides, and oxides. In general, the fabrication of thin films from polymer solid electrolytes is the easiest, yet they often show problems associated with lower mechanical strength and decreased ionic conductivity.[3] Sulfides and oxides offer desirable ionic conductivity and increased mechanical strength, but they are generally difficult to be processed into ultrathin films from bulk materials.

The fabrication of solid electrolytes as ultrathin films is critical to their function because they serve as both the ion transport medium and separator material. When these membranes are too thick, it leads to an increase in the overall volume/mass of the battery and lower power and energy densities, but more critically, it limits the current density that can pass during charging/discharging processes, especially when the solid electrolyte has a low ionic conductivity.[4] It is still challenging to

fabricate thin film solid electrolytes. Typical fabrication methods include radio frequency magnetron sputtering, atomic layer deposition, or pulsed laser deposition.[5] These techniques, however, require expensive and time consuming ultra-high vacuum conditions. Furthermore, controlling the stoichiometry of the thin solid electrolyte films using these techniques can be very difficult, especially for volatile elements such as Li, P, and S.

Sulfide-based solid electrolytes have shown the highest lithium ion conductivity among the three main categories of solid electrolytes for battery-related applications.[6] To this end, $Li_{10}GeP_2S_{12}$ (LGPS) was reported to deliver an ionic conductivity of $\geq 10^{-3}$ $S \cdot cm^{-1}$, comparable to the ionic conductivities of organic liquid electrolyte. However, LGPS is not chemically stable with lithium metal due to the presence of reactive Ge atoms, and the propagation of such chemical reactions limits the electrochemical cycling of the battery. A number of new sulfide-based solid electrolytes have shown relatively high ionic conductivities with necessary compatibility with metallic lithium anodes, e.g., *β*-Li_3PS_4, $Li_7P_2S_8I$, and Li_2S-P_2S_5 glass-ceramics.[7] In general, sulfide-based solid electrolytes are synthesized using solid-state techniques, which require processing at temperatures >400 °C and the use of evacuated ampules, which add to the processing cost of the material. Several sulfide-based solid electrolytes such as *β*-Li_3PS_4, $Li_7P_2S_8I$, and Li_4PS_4I, have recently been synthesized through solvent-based wet-chemical techniques at mild temperatures, offering flexibility in terms of synthesis.[7a, 7b, 8] However, the fabrication of thin films from sulfide-based solid electrolytes is challenging. Although many efforts have been reported, the thickness of sulfide-based solid electrolytes can only be pushed to the range of hundreds of microns to several millimeters.[2a, 9]

In this work, we use sulfide-based *β*-Li_3PS_4 as a model system to demonstrate a novel strategy for significantly reducing the thickness of the solid electrolyte membranes. This technique combines a new synthesis of nanoscale plates with a unique, tiled assembly process that utilizes the

plates as building blocks. Thin films of *β*-Li_3PS_4 with submicron thicknesses have been fabricated. More importantly, the thickness of each building block can be controllably tuned using our method without the degradation of film quality. Comprehensive structural and electrochemical characterizations have also been performed on the thin films. These films hold not only high ionic conductivity but also desirable compatibility with metallic lithium anode. Our results highlight a new, facile strategy for generating ultrathin, dense films of solid electrolytes with desirable ionic conductivities for the next-generation energy storage and conversion systems.

2. Results and Discussion

2.1 Synthesis of the Building Blocks

The fabrication of submicron-thick membranes of *β*-Li_3PS_4 starts with the synthesis of Li_3PS_4·2ACN nanoscale plates, which involves solvent exchange and solution-based exfoliation. We synthesized Li_3PS_4·3THF first using a solvent-based soft chemistry technique by stirring Li_2S and P_2S_5 in anhydrous tetrahydrofuran (THF, C_4H_8O) under argon, using the same procedure as first described by Liu and co-workers.[7a] The Li_2S and P_2S_5 were mixed together at a 3 to 1 molar ratio, and the powder was added into THF under vigorous stirring. After stirring for 24 h, a white precipitate was collected and dried under vacuum at room temperature for 1 h to yield Li_3PS_4·3THF. The Li_3PS_4·3THF was composed of particles with an average size of *ca.* 10 μm (Figure S1). We then fabricated Li_3PS_4·2ACN nanoscale plates by exchanging the co-crystallized THF with ACN by adding 200 mg of the Li_3PS_4·3THF powder in to 100 mL of anhydrous acetonitrile (ACN, C_2H_3N) under vigorous stirring to initiate the process:

$$Li_3PS_4 \cdot 3THF + 2ACN \rightarrow Li_3PS_4 \cdot 2ACN + 3THF$$

After 40 min, the ACN solution changed from white to light blue (Figure S2), indicating the formation of Li_3PS_4·2ACN. During the stirring process, samples were collected at different time points and deposited on silicon wafers for scanning electron microscopy (SEM) imaging. Figure 1A shows an SEM image of the initial Li_3PS_4·3THF powder and Figure 1B-D shows SEM images of the samples after 15 s, 20 min, and 40 min after stirring in ACN. After 15 s, the Li_3PS_4·3THF became exfoliated as evidenced by the formation of sheet-like structures (Figure S3). After 40 min of stirring in ACN, the Li_3PS_4·3THF was converted to Li_3PS_4·2ACN with a well-controlled plate-like morphology, together with a thickness around 80 nm (Figure 2). Energy-dispersive x-ray spectroscopy (EDS) elemental mapping shows that the nanoscale plates contain both S and P (Figure 2C). It is worth noting that directly reacting Li_2S and P_2S_5 in ACN could not produce shape-controlled plate-like building blocks, but rather, irregularly shaped microflakes with a wide size distribution.[4] The procedure based on exchanging the co-crystalized THF with ACN, as explored in the current work, is the key to the successful production of well-defined Li_3PS_4·2ACN rectangular-shaped thin nanoplates that could then serve as building blocks for the fabrication of ultrathin films.

Powder X-ray diffraction (XRD) and Raman spectroscopy confirmed the transformation of Li_3PS_4·3THF to Li_3PS_4·2ACN when the precursor is stirred in ACN (Figure 3). The XRD patterns of Li_3PS_4·3THF and Li_3PS_4·2ACN display distinct peaks that are in good agreement with previous reports.[4, 7a, 7b] The exchange of THF with ACN happens rapidly, with nearly all the coordinated THF being replaced by ACN after about 60 s. After stirring Li_3PS_4·3THF in ACN for 40 min, X-ray diffraction reveals the complete transformation from Li_3PS_4·3THF to Li_3PS_4·2ACN. The exchange of solvent coordination with Li_3PS_4 was further proved by Raman spectroscopy. The initial Li_3PS_4·3THF displayed the characteristic peak for $\nu_s(PS_4)$ at 422 cm^{-1} and C-H vibrations of THF at 2850-3050 cm^{-1} in the Raman spectrum.[7a, 10] After Li_3PS_4·3THF was stirred in ACN for 60 s, a series of spectral changes

occurred, including: *i*) disappearance of C-H vibrations in THF; *ii*) appearance of C≡N stretch for ACN at 2240-2270 cm^{-1}; and iii) appearance of symmetric and asymmetric C-H stretching at 2942-3000 cm^{-1}.[11] These results clearly indicate that Li_3PS_4 prefers to coordinate and co-crystallize with ACN molecules over THF. The appearance of peaks at lower frequencies also confirmed the strong coordination of ACN with lithium ions in Li_3PS_4. Such preferential coordination with ACN could be attributed to the fact that ACN has twice the dipole moment as compared to THF.[12] To evaluate the temperature that was needed to remove the co-crystallized solvent, the phase evolutions of Li_3PS_4·3THF and Li_3PS_4·2ACN upon annealing was monitored using *in situ* XRD. We found that THF could be removed from Li_3PS_4·3THF at a temperature as low as 80 °C, resulting in an amorphous Li_3PS_4 phase, similar to what was described in a previous report.[7a] In comparison, a temperature >180 °C was needed to remove the co-crystallized ACN in Li_3PS_4·2ACN (Figure 3B). It is reasonable to conclude that the relatively high polarity, small size, and steric effects of the ACN molecules are expected to play crucial roles in strongly binding to Li_3PS_4.

Upon solvent removal, the product quickly converted to nanocrystalline orthorhombic *β*-Li_3PS_4 with an average crystallite size ranging from 80 to 120 nm, as derived using the Scherrer equation.[13] Rietveld refinement analysis of *β*-Li_3PS_4 indicated that peak broadening occurs as a result of both the crystallite size and the microstrain (Figure S4). The as-prepared *β*-Li_3PS_4 samples have a microstrain of ~0.12% for an average crystallite size ranging from 80 to 120 nm, which is comparable to the values previously reported *β*-Li_3PS_4 prepared from Li_3PS_4·3THF.[7a] It is worth mentioning that the XRD patterns show that the resultant film was made of pure *β* phase, without the existence of γ phase that gives a lower ionic conductivity.[7a, 10a]

2.2 Fabrication of Solid Electrolyte Membranes

Thin membranes of *β*-Li_3PS_4 solid electrolyte were fabricated using a novel three-step processing method, involving *i*) assembly of the nanoscale solid electrolyte building blocks, *ii*) decomposition of Li_3PS_4·2ACN to *β*-Li_3PS_4, and *iii*) fusion of the solid electrolyte building blocks. By taking advantage of the solvent exchange mechanism, thin films of plate-like Li_3PS_4·2ACN building blocks were first dispersed on Ni substrates by tiled assembly, similar to what is used in evaporation-induced self-assembly (EISA), where solvent removal through evaporation directs the deposition of solid electrolyte particles.[4, 14] The tiled assembly of plate-like Li_3PS_4·2ACN building blocks relies on their well-defined aspect ratios, such that the nanoscale building blocks stack face-to-face as thin films during deposition. In a typical process, polished Ni substrates were dipped into a suspension of plate-like Li_3PS_4·2ACN building blocks in ACN with a specific concentration (e.g., 0.01–0.8 M), followed by a heat treatment at 80 °C to remove the excess solvent. As shown by the SEM images, the surface of the Li_3PS_4·2ACN nanoscale building blocks maintained their rectangular, flaky morphology after heating to 80 °C and uniform films were produced (Figure S4). The key to making ultrathin films is to directly disperse suspensions of Li_3PS_4·2ACN building blocks on substrates. In order to improve the ionic conductivity of these Li_3PS_4 thin films, the remaining co-crystalized ACN must be removed. As evidenced by XRD patterns of Li_3PS_4·2ACN, a temperature of greater than 180 °C was necessary to remove the co-crystallized ACN and produce *β*-Li_3PS_4. After warm pressing at 200 °C and 200 MPa for 15 min, the particles in the *β*-Li_3PS_4 thin films fused together, yielding dense solid electrolyte membranes. Freestanding membranes were obtained by carefully peeling the polished Ni foil from the surface of the *β*-Li_3PS_4 thin film (see experimental for details).

An interesting discovery in this work was that the thickness of the *β*-Li_3PS_4 solid electrolyte films could be readily tailored by tuning the concentration of the Li_3PS_4·2ACN nanoscale building

blocks in ACN between 0.01 and 0.8 M, and more importantly, the thickness of these films could be pushed all the way down to the submicron scale. Figure 4 shows SEM images of the warm-pressed solid electrolyte membranes fabricated from suspensions of Li_3PS_4·2ACN building blocks with different concentrations. Tuning the concentration of Li_3PS_4·2ACN in ACN from 0.1 to 0.8 M allowed for the fabrication of micron-thick membranes ranging from 6 to 35 µm. When the concentration of Li_3PS_4·2ACN building blocks was further reduced to 0.01 M, we obtained a submicron-thick solid electrolyte film of *β*-Li_3PS_4 after warm pressing at 200 °C, which was measured to be 0.4 µm in thickness, making it among the thinnest reported for warm-pressed sulfide-based solid electrolyte films. Figure 4A shows an SEM image of the cross section of the 0.4 µm *β*-Li_3PS_4 membrane, implying that the warm-pressed membrane was comprised of 4-5 layers of the plate-like, nanoscale building blocks. Figure 4B displays an SEM image of the surface of the *β*-Li_3PS_4 membrane, indicating that most of the flakes had fused together to form a dense, continuous membrane. After warm pressing at 200 °C, the membranes achieved densities between 95-98% of the reported bulk *β*-Li_3PS_4 material, implying that the warm-pressed membranes have a porosity of 2-5%. Similar densities were achieved with glassy sulfides, but the glassy sulfide membranes were generally much thicker than those highlighted in the current report.[15]

2.3 Electrochemical Performance of *β*-Li_3PS_4 Membranes

The ionic conductivity of the newly formed membranes were studied using electrochemical impedance spectroscopy. Figure 5 shows a representative comparison of Nyquist and derived Arrhenius plots of Li_3PS_4·2ACN and the *β*-Li_3PS_4 films after warm pressing. Li_3PS_4·2ACN show a larger diameter in the semicircle of the Nyquist plot (Figure 5A), indicating a lower conductivity. This can be explained by the presence of solvent molecules, which lowers the Li^+ mobility. Upon the removal of

ACN, the thin β-Li_3PS_4 membranes exhibited an average AC ionic conductivity of 7.2×10^{-5} S·cm^{-1} at 20 °C (Table S1), an improvement of four orders of magnitude over the Li_3PS_4·2ACN (Figure 5). Additionally, the total observed ionic conductivity displayed an Arrhenius behavior between 20 and 100 °C according to the following relationship (Equation 1):

$$\sigma = \sigma_o \cdot e^{\frac{-E_a}{kT}} \quad (1)$$

where σ_o denotes the temperature independent ionic conductivity of the film, *k* represents the Boltzmann constant, and E_a denotes the activation energy. The Arrhenius activation energy of Li_3PS_4·2ACN and β-Li_3PS_4 were determined to be 0.69 eV and 0.36 eV, respectively.[4, 7a, 7d] It should be noted that the activation energy of our β-Li_3PS_4 thin film is lower than that of bulk β-Li_3PS_4, which was reported to be ~0.46 eV.[10a] Such an enhancement can be attributed to *i*) the desired phase purity, *i.e.* no impurity phases such as the γ phase, $Li_4P_2S_6$, or $Li_{3.2}P_{0.96}S_4$,[16] and *ii*) the small grain size that gives a larger concentration of grain boundaries concentrations along which Li^+ may have a higher mobility.[7a]

The compatibility of the β-Li_3PS_4 thin film with metallic lithium was evaluated using a symmetric cell configuration (Li/β-Li_3PS_4/Li) with direct current (DC) polarization. Such configuration allows for the evaluation of interfacial stability through resistance measurements.[17] As shown in Figure 6, the solid electrolyte membranes adopted in the present work could be cycled hundreds of times at current density between 0.1 and 0.3 mA·cm^{-2}. The ionic conductivity from DC polarization was 6.8×10^{-5} S·cm^{-1} at 20 °C, which is comparable to the AC ionic conductivity of 7.2×10^{-5} S·cm^{-1} at 20 °C, signifying that the conductivity mainly originates from lithium ions in the thin β-Li_3PS_4 solid electrolyte membranes. This result is comparable with that of the previously reported β-Li_3PS_4 and Li_2S-P_2S_5 glass-ceramics,[7a, 7d, 7e] indicating that the thin film does not experience propagating chemical reactions with lithium metal. A slight increase in the interfacial resistance was observed in

the first 3000 min (Figure 6), possibly due to the formation of a passivation layer and/or lithium redistribution at the interface. Similar results were also obtained with thin β-Li_3PS_4 solid electrolyte membranes of other thicknesses in the range of 0.4−28 μm, as shown in Figure S7. After cycling over 500 times (Figure S8), the resistance from DC polarization did not increase significantly, suggesting the desired interfacial stability of Li/β-Li_3PS_4 thin film during electrochemical cycling. As the increase in interfacial resistance happened at the beginning and became stable upon long-term cycling, it is most likely that an interphase layer that is electronically insulating forms at the interface and in turn prevents the propagation of chemical transformations at the interface. In fact, as predicted by theory, it is possible that β-Li_3PS_4 decomposes to Li_3P and Li_2S due to its electrochemical instability to metallic lithium, however, the decomposed interface layer is often self-limiting and capable of passivating further interfacial reactions.[18] Such a phenomenon is not rare and has been experimentally observed[7a, 19] and theoretically predicted[20] in multiple solid electrolyte materials.

3. Conclusion

In summary, we have demonstrated a new approach to the fabrication of ultrathin solid electrolyte membranes for all-solid-state batteries. This technique combines a new synthesis strategy for generating shape-controlled nanoplates of Li_3PS_4·2ACN with a unique tiled assembly process that utilizes these nanoplates as building blocks to produce submicron thin membranes. This method offers the flexibility of synthesizing thin films with desired thicknesses in a controlled way. Ultrathin β-Li_3PS_4 membranes of less than 0.5 μm in thickness were fabricated for the first time. Apart from the desirable thickness, the ultrathin β-Li_3PS_4 films also hold additional advantages: increased ionic conductivity, a decreased Arrhenius activation energy compared with bulk Li_3PS_4, and good electrochemical compatibility with metallic lithium anode. This new solution-based soft

chemistry method offers the flexibility of fabricating ultrathin solid electrolyte membranes for the next-generation of energy storage and conversion devices.

4. Experimental Section

Synthesis of Materials: Lithium sulfide (Li_2S, Alfa Aesar, 99.9%) and phosphorus pentasulfide (P_2S_5, Sigma-Aldrich, 99%) were mixed with a stoichiometry of 3 to 1 in anhydrous tetrahydrofuran (THF, Sigma-Aldrich, >99.8%) at room temperature. After stirring for 24 h, a white precipitate was observed. The precipitate was collected by filtration and dried at room temperature under vacuum for 1 h to remove excess solvent, yielding $Li_3PS_4 \cdot 3THF$. In the next step, 200 mg of the as-obtained $Li_3PS_4 \cdot 3THF$ was added into 100 mL of anhydrous acetonitrile (ACN, Sigma-Aldrich, >99.8%) and stirred vigorously. A drop of the suspension was deposited on a Si substrate and dried under vacuum at room temperature to monitor the morphology variation after stirring for 15 s, 1 min, 5 min, 10 min, 20 min, 40 min, 60 min, and 24 h, respectively. The final product was collected by filtration and then heated at 80 °C to produce $Li_3PS_4 \cdot 2ACN$. Considering the sensitivity of the system to O_2 and moisture, all the experiments were carried out in an Argon-filled glove box.

Characterization of Materials: SEM images were collected on a field-emission scanning electron microscope (SEM, Zeiss Merlin) at an acceleration voltage of 5.0 kV equipped with a custom designed stage for handling air-sensitive samples.[21] Identification of the crystalline phase was conducted on a X'pert Pro Powder Diffractometer (PANalytical) with Cu Kα radiation. All XRD samples were prepared in a glovebox and the quartz slides were sealed with Kapton® films. Rietveld refinement was performed with HighScore Plus, a software package provided by PANalytical. Raman

spectra of Li_3PS_4·3THF, the intermediate, and Li_3PS_4·2ACN were collected on an Acton Trivista 555 spectrometer (Princeton Instruments).

Fabrication of Membranes: Thin membranes of *β*-Li_3PS_4 were fabricated using the Li_3PS_4·2ACN plates by following our previous report.[4] Simply put, a suspension of Li_3PS_4·2ACN plates was prepared by dispersing Li_3PS_4·2ACN plates in a beaker containing ACN. The concentration of Li_3PS_4·2ACN plates was tuned between 0.01–0.8 M to create membranes with varying thicknesses. Polished Ni substrates were dipped into the Li_3PS_4·2ACN suspensions, placed on a horizontal surface, transferred into a chemical dryer, and heated under vacuum at 80 °C to remove excess solvent. The membranes were then warm pressed at a temperature of 200 °C at 200 MPa between two nickel substrates for 15 min. Freestanding thin films of *β*-Li_3PS_4 were obtained by carefully peeling the polished Ni foil from the surface of the solid electrolyte after warm pressing. All processes were completed under Argon due to the sensitivity of Li_3PS_4 to moisture and air.

Electrochemical Measurements and Fabrication of All-Solid-State Batteries: Swagelok® cells were used to complete all electrochemical impedance spectroscopy (EIS), cyclic voltammetry (CV) and cycling performance measurements. For EIS, films were prepared between two carbon-coated Al foils and measured between 1 MHz and 1 mHz at an amplitude of 100.0 mV. For the CV tests, Li/*β*-Li_3PS_4/Pt cells were scanned at a rate of 0.1 mV·s^{-1} between -0.5 and 5 V *vs.* Li/Li^+ at room temperature using a Bio-Logic VSP multi-channel potentiostat. The Li/*β*-Li_3PS_4/Li symmetric cells were cycled on a battery system (Bio-Logic VSP) at current densities of 0.1 and 0.3 mA·cm^{-2}.

Supporting Information

Supporting Information is available from the Wiley Online Library or from the author.

Acknowledgements

This work was completed at the Center for Nanophase Materials Sciences, which is a DOE Office of Science User Facility. This work was also sponsored by the U.S. Department of Energy (DOE), Office of Science, Basic Energy Sciences, Materials Sciences and Engineering Division. The authors thank Nancy J. Dudney for helpful discussions and critique of the manuscript. Z.D.H. gratefully acknowledges support from the National Science Foundation Graduate Research Fellowship under Grant No. DGE-1650044 and the Georgia Tech-ORNL Fellowship. H.W. thanks the support from NSF EPSCoR Grant (Grant No. 1355438), Conn Center for Renewable Energy Research, and EVPRI Internal Grants from the University of Louisville.

References

[1] a) W. Xu, J. Wang, F. Ding, X. Chen, E. Nasybulin, Y. Zhang, J.-G. Zhang, *Energy Environ. Sci.* **2014**, *7*, 513-537; b) Y. Guo, H. Li, T. Zhai, *Advanced Materials* **2017**; c) D. Lin, Y. Liu, Y. Cui, *Nat. Nanotechnol.* **2017**, *12*, 194-206.

[2] a) Z. Lin, C. Liang, *J. Mater. Chem. A* **2015**, *3*, 936-958; b) N. J. Dudney, W. C. West, J. Nanda, *Handbook of Solid State Batteries*, World Scientific, **2016**.

[3] D. T. Hallinan Jr, N. P. Balsara, *Annu. Rev. Mater. Res.* **2013**, *43*, 503-525.

[4] H. Wang, Z. D. Hood, Y. Xia, C. Liang, *J. Mater. Chem. A* **2016**, *4*, 8091-8096.

[5] a) E. Quartarone, P. Mustarelli, *Chem. Soc. Rev.* **2011**, *40*, 2525-2540; b) Y. Ito, A. Sakuda, T. Ohtomo, A. Hayashi, M. Tatsumisago, *J. Ceram. Soc. Jpn.* **2014**, *122*, 341-345.

[6] a) J. C. Bachman, S. Muy, A. Grimaud, H.-H. Chang, N. Pour, S. F. Lux, O. Paschos, F. Maglia, S. Lupart, P. Lamp, *Chem. Rev.* **2015**, *116*, 140-162; b) Y. Wang, W. D. Richards, S. P. Ong, L. J. Miara, J. C. Kim, Y. Mo, G. Ceder, *Nat. Mater.* **2015**.

[7] a) Z. Liu, W. Fu, E. A. Payzant, X. Yu, Z. Wu, N. J. Dudney, J. Kiggans, K. Hong, A. J. Rondinone, C. Liang, *J. Am. Chem. Soc.* **2013**, *135*, 975-978; b) E. Rangasamy, Z. Liu, M. Gobet, K. Pilar, G. Sahu, W. Zhou, H. Wu, S. Greenbaum, C. Liang, *J. Am. Chem. Soc.* **2015**, *137*, 1384-1387; c) E. Rangasamy, G. Sahu, J. K. Keum, A. J. Rondinone, N. J. Dudney, C. Liang, *J. Mater. Chem. A* **2014**, *2*, 4111-4116; d) Z. D. Hood, H. Wang, Y. Li, A. S. Pandian, M. P. Paranthaman, C. Liang, *Solid State Ionics* **2015**, *283*, 75-80; e) A. Hayashi, S. Hama, F. Mizuno, K. Tadanaga, T. Minami, M. Tatsumisago, *Solid State Ionics* **2004**, *175*, 683-686.

[8] S. J. Sedlmaier, S. Indris, C. Dietrich, M. Yavuz, C. Dräger, F. von Seggern, H. Sommer, J. Janek, *Chem. Mat.* **2017**, *29*, 1830-1835.

[9] a) R. Murugan, V. Thangadurai, W. Weppner, *Angew. Chem. Int. Ed.* **2007**, *46*, 7778-7781; b) S. Teragawa, K. Aso, K. Tadanaga, A. Hayashi, M. Tatsumisago, *J. Mater. Chem. A* **2014**, *2*, 5095-5099; c) T. Yamada, S. Ito, R. Omoda, T. Watanabe, Y. Aihara, M. Agostini, U. Ulissi, J. Hassoun, B. Scrosati, *J. Electrochem. Soc.* **2015**, *162*, A646-A651; d) P. Bron, S. Johansson, K. Zick, J. r. Schmedt auf der Günne, S. Dehnen, B. Roling, *J. Am. Chem. Soc.* **2013**, *135*, 15694-15697.

[10] a) M. Tachez, J.-P. Malugani, R. Mercier, G. Robert, *Solid State Ionics* **1984**, *14*, 181-185; b) N. Machida, H. Yamamoto, S. Asano, T. Shigematsu, *Solid State Ionics* **2005**, *176*, 473-479; c) B. Cadioli, E. Gallinella, C. Coulombeau, H. Jobic, G. Berthier, *J. Phys. Chem.* **1993**, *97*, 7844-7856.

[11] K. Tanabe, *Chem. Phys.* **1979**, *38*, 125-129.

[12] V. I. Minkin, *Dipole Moments in Organic Chemistry*, Springer Science & Business Media, **2012**.

[13] a) K. Homma, M. Yonemura, T. Kobayashi, M. Nagao, M. Hirayama, R. Kanno, *Solid State Ionics* **2011**, *182*, 53-58; b) K. Momma, F. Izumi, *J. Appl. Crystallogr.* **2011**, *44*, 1272-1276.

[14] a) C. J. Brinker, Y. Lu, A. Sellinger, H. Fan, *Adv. Mat.* **1999**, *11*, 579-585; b) D. Grosso, F. Cagnol, G. d. A. Soler-Illia, E. L. Crepaldi, H. Amenitsch, A. Brunet-Bruneau, A. Bourgeois, C. Sanchez, *Adv. Funct. Mat.* **2004**, *14*, 309-322.

[15] a) H. Kitaura, A. Hayashi, T. Ohtomo, S. Hama, M. Tatsumisago, *J. Mater. Chem.* **2011**, *21*, 118-124; b) Y. Seino, T. Ota, K. Takada, A. Hayashi, M. Tatsumisago, *Energy Environ. Sci.* **2014**, *7*, 627-631.

[16] a) Z. D. Hood, C. Kates, M. Kirkham, S. Adhikari, C. Liang, N. Holzwarth, *Solid State Ionics* **2016**, *284*, 61-70; b) K. Minami, A. Hayashi, M. Tatsumisago, *J. Cer. Soc. Jpn.* **2010**, *118*, 305-308.

[17] a) J. Burns, L. Krause, D.-B. Le, L. Jensen, A. Smith, D. Xiong, J. Dahn, *J. Electrochem. Soc.* **2011**, *158*, A1417-A1422; b) Y. Tian, T. Shi, W. D. Richards, J. Li, J. C. Kim, S.-H. Bo, G. Ceder, *Energy Environ. Sci.* **2017**, *10*, 1150-1166.

[18] a) N. Lepley, N. Holzwarth, *Phys. Rev. B* **2015**, *92*, 214201; b) N. Lepley, N. Holzwarth, Y. A. Du, *Phys. Rev. B* **2013**, *88*, 104103.

[19] a) C. Ma, Y. Cheng, K. Yin, J. Luo, A. Sharafi, J. Sakamoto, J. Li, K. L. More, N. J. Dudney, M. Chi, *Nano Lett.* **2016**; b) A. Schwöbel, R. Hausbrand, W. Jaegermann, *Solid State Ionics* **2015**, *273*, 51-54; c) Z. D. Hood, H. Wang, A. Samuthira Pandian, J. K. Keum, C. Liang, *J. Am. Chem. Soc.* **2016**, *138*, 1768-1771; d) J. Howard, Z.D. Hood, N.A.W. Holzwarth, *Phys. Rev. Mater.* **2017**, *1*, 075406; e) L. E. Rush, Z. D. Hood, N. A. W. Holzwarth, *Phys. Rev. Mater.* **2017**, *1*, 075405; f) H. Wang, Y. Chen, Z. D. Hood, G. Sahu, A. S. Pandian, J. K. Keum, K. An, C. Liang, *Angew. Chem. Int. Ed.* **2016**, *55*, 8551-8555.

[20] a) Y. Zhu, X. He, Y. Mo, *J. Mater. Chem. A* **2016**, *4*, 3253-3266; b) W. D. Richards, L. J. Miara, Y. Wang, J. C. Kim, G. Ceder, *Chem. Mat.* **2015**, *28*, 266-273.

[21] J. Y. Howe, L. A. Boatner, J. A. Kolopus, L. R. Walker, C. Liang, N. J. Dudney, C. R. Schaich, *J. Mater. Sci.* **2012**, *47*, 1572-1577.

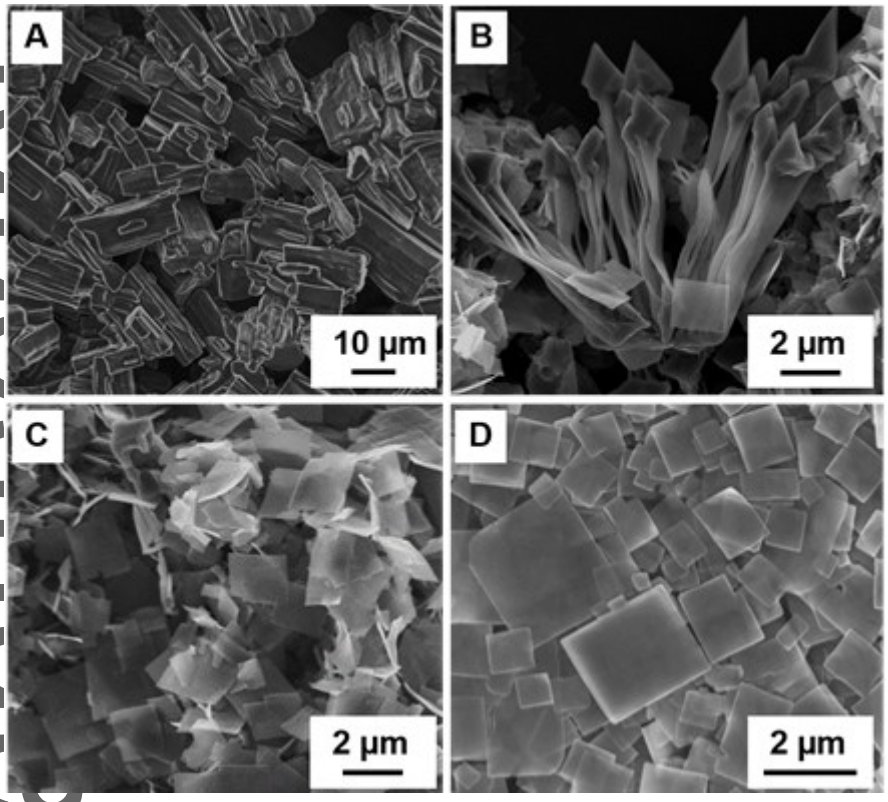

Figure 1. SEM images of Li_3PS_4·3THF (A) before and (B-D) after stirring in ACN for B) 15 s, C) 20 min, and D) 40 min. During this process, well-defined plates of Li_3PS_4·2ACN were precipitated out from the reaction solution.

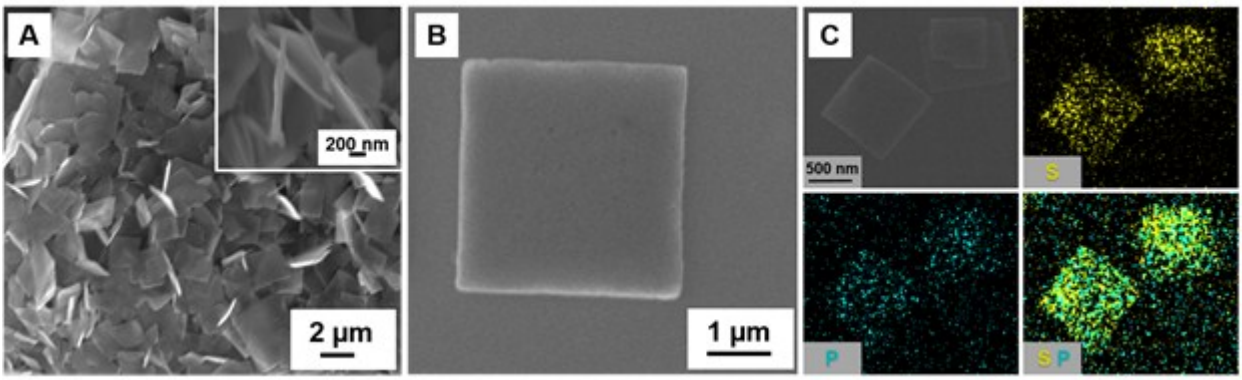

Figure 2. A, B) SEM images of plate-like, nanoscale building blocks of Li_3PS_4·2ACN at different magnifications. The inset shows a side-view image of some plates, revealing a thickness of around 80 nm for the individual Li_3PS_4·2ACN plates. C) SEM image and EDS elemental mapping of nanoscale plates of Li_3PS_4·2ACN, showing uniform distributions of phosphorus and sulfur across the Li_3PS_4·2ACN plates.

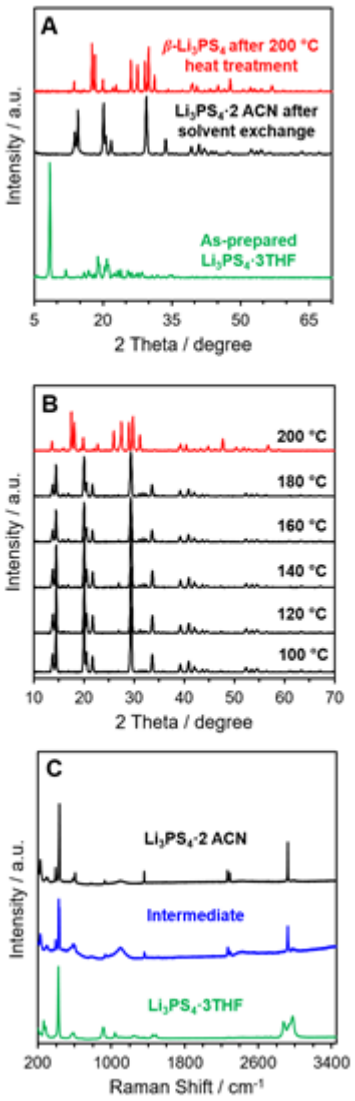

Figure 3. A) XRD patterns of the as-prepared Li_3PS_4·3THF, Li_3PS_4·2ACN (after solvent exchange and drying at 80 °C), and *β*-Li_3PS_4 (after heating Li_3PS_4·2ACN at 200 °C). B) XRD patterns after heating Li_3PS_4·2ACN at different temperatures, showing that a temperature of 200 °C is critical to the removal of ACN and thus formation of *β*-Li_3PS_4. C) Raman spectra taken from Li_3PS_4·3THF (an intermediate) and Li_3PS_4·2ACN. The solvent exchange process started to occur in less than 60 s, indicating that Li_3PS_4 preferentially coordinates with ACN.

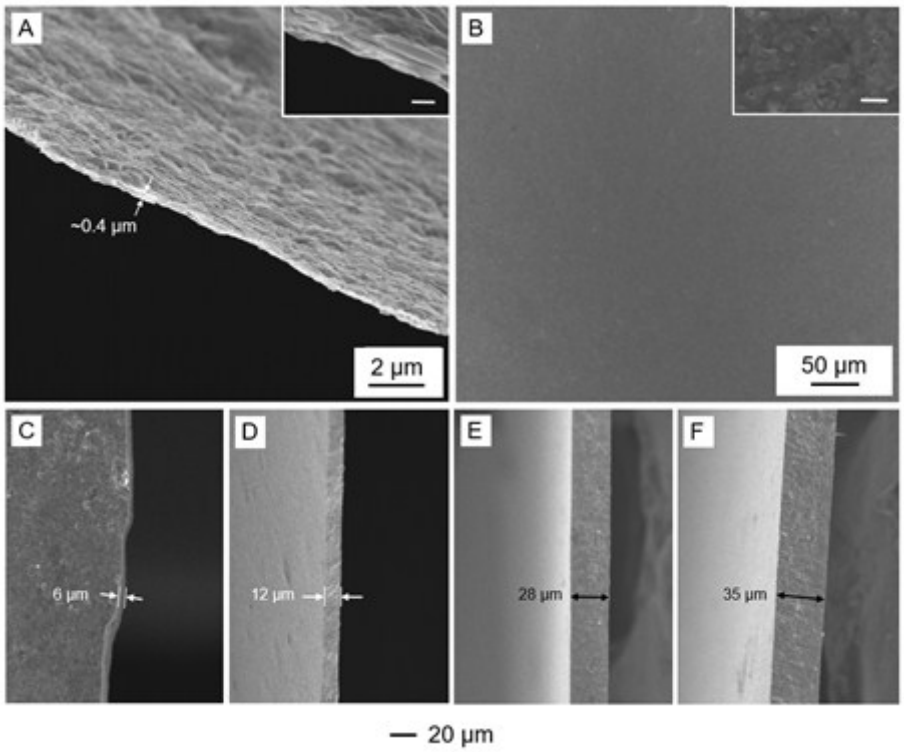

Figure 4. SEM images of the A) cross section and B) top surface of a *β*-Li_3PS_4 ultrathin film with a thickness of 0.4 µm after warm pressing at 200 °C (inset scale bars: 100 nm). C-F) SEM images of *β*-Li_3PS_4 thin films with thicknesses varying from 6 to 35 µm after warm pressing at 200 °C.

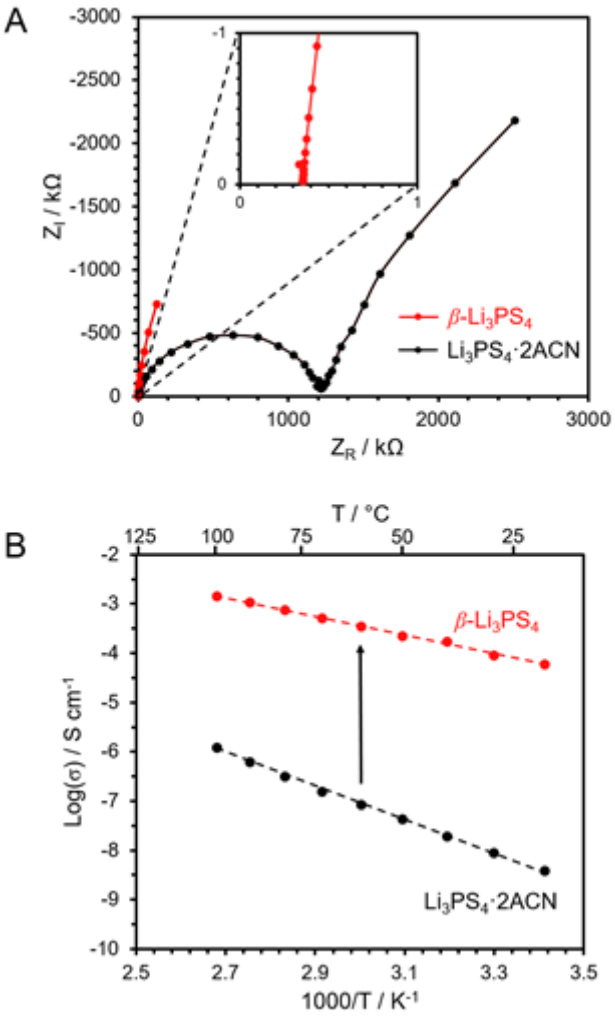

Figure 5. A) Nyquist and B) Arrhenius plots for representative films of Li_3PS_4·2ACN and the *β*-Li_3PS_4 derived from the Li_3PS_4·2ACN with a thickness of 12 µm. The Nyquist plots in (A) were both collected at 25 °C.

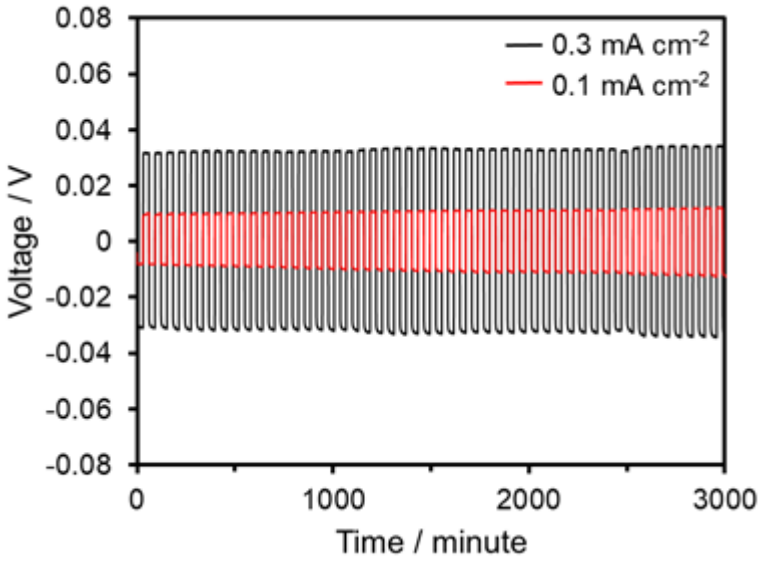

Figure 6. Electrochemical stability of an ultrathin film of *β*-Li_3PS_4 with a thickness of 12 µm in contact with metallic lithium. Representative cycling data of a Li/*β*-Li_3PS_4/Li symmetric cell at current densities of 0.1 mA·cm^{-2} and 0.3 mA·cm^{-2}, respectively, at 25 °C. The full cycling profile over 500 cycles is shown in Figure S5.